Phuong Vu[1], Quan Nguyen[2], Minh Tran[1], Duong Tuan[1,3], Hung Tran[1]

J. Electrical Systems 14-4 (2018): 102-115

Regular paper

Journal of Electrical Systems

A systematic design of PR current controllers for single-phase LCL-type grid-connected inverters under distorted grid voltage

LCL-type grid-connected inverters are crucial for the integration of distributed energy resources in power grids. In order to achieve high quality of the grid current for a compliance with IEEE and IEC standards and maintain system stability, not only an LCL resonance damping method but also a proper controller design is required. This paper proposes a systematic and generalized design approach for PR controllers to stabilize the operation of single-phase LCL-type grid-connected inverters under different conditions of grid voltage. The designed PR controller contains multiple resonant components to effectively eliminate high-order current harmonics and deal with the variation of grid frequency. Phase margin is taken into account when designing the PR controller to guarantee system stability. The efficacy of the proposed method is verified by both simulation and real-time hardware-in-the-loop experiments using a Typhon HIL 402 system. The results show that the designed PR current controller is capable of significantly reducing grid-current harmonics when the system operates with distorted grid voltage. In addition, between grid-current and inverter-current feedback approaches, the former results in a grid current with a higher quality.

Keywords: PR controller, LCL filter, Grid-connected inverter.

Article history: Received 23 February 2018, Accepted 8 November 2018

1. Introduction

Nowadays voltage source inverters (VSI) are an essential components for the rapid integration of distributed energy resources to electrical power grids. Traditional VSIs are connected to the grid by means of a single inductor L to reduce ripple currents resulted from the harmonic components at switching frequencies. The main limitation of L filters is the poor harmonic alleviation due to its first-order transfer function. Therefore, LCL filters with third-order transfer function have recently been attracting much interest because of their superior capability in attenuating harmonics, fast dynamic responses, and smaller sizes and weights compared to L filters [1]-[3]. The structure of an LCL-type grid-connected VSI system is shown in Fig. 1.

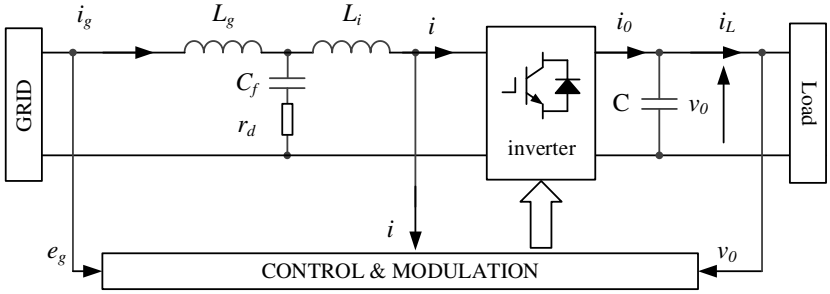

Figure 1. Block diagram of a grid-connected inverters with LCL filter.

In spite of these advantageous properties, LCL filters introduce a resonance caused by a zero impedance at a high-order frequency. As a result, the current harmonics around this frequency might be considerable, which degrades the quality of the output current [1]-[7].

* Corresponding author: Phuong Vu, School of Electrical Engineering, Hanoi University of Science and Technology, Hanoi, Vietnam, Email: phuong.vuhoang@hust.edu.vn

[1] School of Electrical Engineering, Hanoi University of Science and Technology, Hanoi, Vietnam

[2] Department of Electrical and Computer Engineering, The University of Texas at Austin, Texas, U.S.A

[3] Hanoi University of Industry, Hanoi, Vietnam

Therefore, advanced improvements in both hardware and control are required to reduce this undesired sensitivity of LCL-type grid-connected VSIs to grid distortion. The proposed improvements to suppress the LCL filters resonance in grid-connected VSIs can be classified into passive and active damping approaches [4],[5],[7]-[12]. The passive damping method, which involves hardware modifications with additional passive components, is easier and cheaper to implement for stiff-grid applications. The feedback current can be either inverter current or grid current. However, this approach comes with the expense of extra losses, and it might affect the high-frequency harmonic attenuation capability [4]. On the contrary, active damping has no additional power losses since it makes changes in the control strategies. Active damping can be realized by either placing an auxiliary filter in the control loop or implementing single- or multi-loop current control [4],[5],[7]-[10]. The state-feedback signals in the later are either inverter and grid currents or capacitor and grid currents, both have been shown to achieve similar dynamic performances [5]-[8]. Despite the complexity and high overall cost due to an additional number of sensors, active damping has been widely used since they are more effective and flexible in stabilizing the system [5].

The quality of the injected grid current is of great importance in grid-connected VSIs. Therefore, choosing a proper controller for control loops is as crucial as selecting a good damping method. The conventional and popular PI controllers suffer from the presence of steady-state errors in single-phase applications, poor disturbance rejection capability, and the need for transformation from and to the synchronously rotating frame [10],[11], [13]-[17]. Recently, PR controllers have been suggested as an alternative option for PI controllers in grid-connected VSI applications. PR controllers have an infinite gain at a selected resonant frequency; thus, the zero steady-state error or the harmonic at this frequency can be eliminated [10],[13]-[14]. PR controllers are flexible to works with both positive- and negative-sequence components, and they are implemented directly in the stationary frame [13]. The main disadvantage of PR controllers is that they are sensitive to the variation of the selected frequency; that is, a small variation at that frequency might prevent the PR controller from precisely tracking the reference signal [10],[12]. However, PR controllers are still theoretically the better choice for single-phase grid-connected VSIs compared to the conventional PI controllers in general.

To obtain the parameters of PR controllers in LCL-type grid-connected, several existing works consider a reduced model of LCL filter as a first-order transfer function. This simplification reduces the quality of the current loop in terms of the transient time, overshoot, and system stability since the exact model of LCL filter is a third-order transfer function. Another approach to design PR controllers is based on the SISO design tool in MATLAB and system dynamic response [16], which is time-consuming and not generalized. More importantly, most of existing works focus on determining PR parameters only for a single harmonic frequency, which is usually the fundamental frequency [10],[13]-[16]. In [17], although the authors address to the PR controllers containing multiple resonant components to deal with grid voltage harmonic, the variation of the grid frequency is not included. In such a scenario, a non-ideal PR controllers must be used.

This paper proposes a systematic and generalized design method for PR current controllers in LCL-type grid-connected VSIs. The major advantageous properties of the proposed method include:

- A non-ideal PR controller that contains multiple resonant components to eliminate the effect of grid voltage harmonics and the variation of the fundamental grid frequency. The proposed non-ideal PR controller is thus suitable for different operating conditions of the grid.

- The parameters of the PR controller are designed in the frequency domain, taking into account the full third-order model of LCL filters and the desired limits of system phase margin, which guarantees system stability. The discretization in the z-domain of the designed PR controller for digital implementation is also included.
- The proposed method is applicable for both of inverter-current and grid-current feedback control schemes. Therefore, it is able to improve the quality of grid-connected VSIs with both passive and active damping approaches.
- The efficacy of the proposed method is verified by both simulation and hardware-in-the-loop (HIL) real-time experiments using a Typhoon HIL 402 system.

The remaining paper is organized as follows. Section 2 includes the notations used in this paper. Section 3 describes the full third-order model of LCL-type VSIs, the transfer functions of the ideal and non-ideal PR controllers, and the proposed design in the frequency domain of the non-ideal PR current controller in grid-connected systems with distorted grid voltage. The discretization of the designed PR controller is also included. Section 4 demonstrates the efficacy of the proposed method by off-line simulations and hardware-in-the-loop (HIL) real-time experiments.

2. Notation

The notations used throughout the paper are stated below.

Indexes:

PR	Proportional resonant
PM	Phase margin
THD	Total Harmonic Distortion
SRF	Synchronous rotation frame
$G_{vi_s}(s)$	The transfer function from inverter-side voltage to inverter-side current
$G_{vi_g}(s)$	The transfer function from inverter-side voltage to grid-side current
$G_{PR}(s)$	The transfer function of proportional resonant (PR) controller in s domain
$G_R^d(z)$	The proportional resonant (PR) controller design in discrete domain
$G_{PI}^+(s)$	The positive sequence transfer functions of the classic PI controller in the SRF
$G_{PI}^-(s)$	The negative sequence transfer functions of the classic PI controller in the SRF

3. The proposed design methodology for non-ideal PR current controllers

3.1. Design of parameters for non-ideal PR controllers

In grid-connected VSIs, an L filter or an LCL filter is usually used as the interface between the inverter and the grid to eliminate excessive switching ripples of grid current because of the pulse-width modulation (PWM) process. An LCL filter has better attenuation capacity of the switching harmonics and better dynamic characteristics than those of an L filter. Nevertheless, the transfer function of LCL filter is a third-order system, and instability problems may occur at the resonant frequency. A passive resistor is thus inserted in the capacitor of the LCL filter to damp the LCL filter resonance. The model of an LCL filter with passive damping is shown in Fig. 2. The transfer functions of the inverter-side current i_s and grid-side current i_g to the inverter-side voltage with the damping resistor are given as follows:

$$G_{vi_s}(s) = \left.\frac{i_s(s)}{v_s(s)}\right|_{e_n=0} = \frac{1}{L_i s}\frac{\left(s^2 + r_d C_f z_{LC}^2 s + z_{LC}^2\right)}{\left(s^2 + r_d C_f \omega_{res}^2 s + \omega_{res}^2\right)} \tag{1}$$

$$G_{vi_g}(s)=\left.\frac{i_g(s)}{v_s(s)}\right|_{e_n=0}=\frac{1}{L_i s}\frac{1+r_d C_f s}{\left(s^2+r_d C_f \omega_{res}^2 s+\omega_{res}^2\right)} \tag{2}$$

where $z_{LC}^2=\left[L_g C_f\right]^{-1}$, $\omega_{res}^2=\left(L_g+L_i\right)z_{LC}^2/L_i$, and ω_{res} is the resonance frequency of the LCL filter. The frequency responses of these transfer functions are shown in Fig. 3.

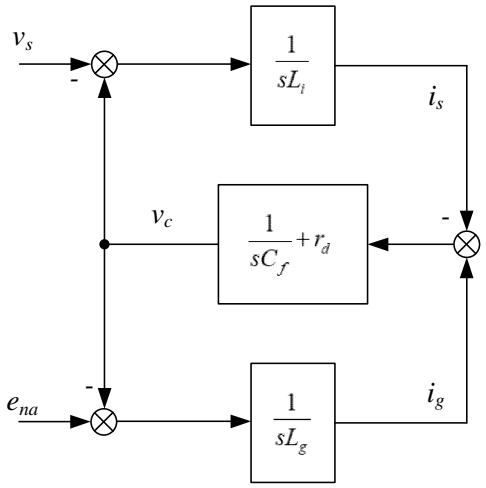

Figure 2. Model of LCL filter with passive damping.

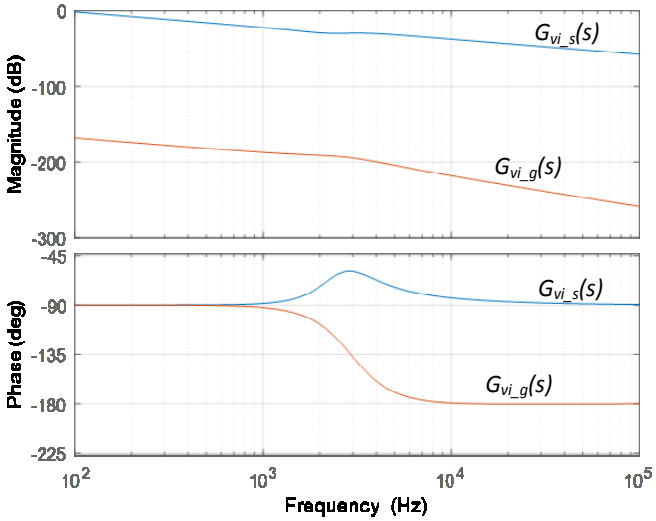

Figure 3. Responses in the frequency domain of $G_{vi_s}(s)$ and $G_{vi_g}(s)$ with the chosen parameteres shown in Table 1.

The proportional resonant (PR) controller provides gains at a certain frequency (resonant frequency) and eliminates steady-state errors. Therefore, the PR controller can be successfully applied to single-phase grid-connected VSIs. The transfer function of an ideal PR controller is given as follows:

$$G_{PR}(s)=K_{ph}+\frac{K_{rh}s}{s^2+\omega_h^2} \tag{3}$$

Where K_{ph}, K_{rh}, and ω_h are the proportional gain, resonant gain, and frequency for the *h*-order harmonic, respectively. However, in practical application, the infinite gain associated with the ideal case might lead to instability problems. Therefore, a non-ideal PR controller given as follows is applied to improve the performance of the controlled system:

$$G_{PR}(s)=K_{ph}+\frac{2K_{rh}\omega_{PRc}s}{s^2+2\omega_{PRc}s+\omega_h^2} \tag{4}$$

With ω_{PRc} being the bandwidth at -3dB cutoff frequency of the controller to reduce the sensitivity toward frequency variation in grid power, the gain of the controller at $\left(\omega_h\pm\omega_{PRc}\right)$ is approximated to $K_{rh}/\sqrt{2}$ [15]. Examples of Bode diagram of several PR controllers with the fundamental resonant frequency are shown in Fig. 4. In this practice, K_{ph} is set to 1, K_{rh} is set to 100, 1000, and 10000, respectively, and $\omega_{PRc}=2\pi$ rad/s.

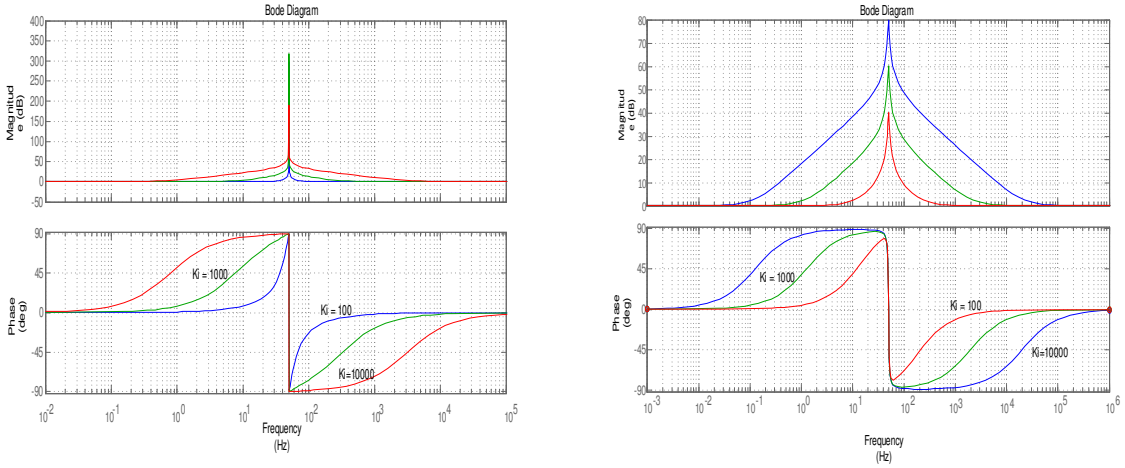

Figure 4. Bode diagrams of PR controllers with the fundamental resonant frequency.

The frequency response characteristics of the non-ideal PR controller at the selected resonant frequency are calculated as follows:

$$\left|G_{PR}(j\omega)\right| = \frac{\sqrt{K_{ph}^2\left(\omega_h^2-\omega^2\right)^4+\left(\omega_h^2-\omega^2\right)^2\left(\omega_{PRc}\omega\right)^2\left(8K_{ph}^2+8K_{ph}K_{rh}+4K_{rh}^2\right)+16\left(\omega_{PRc}\omega\right)^4\left(K_{ph}+K_{rh}\right)^2}}{\left(\omega_h^2-\omega^2\right)^2+4\left(\omega_{PRc}\omega\right)^2} \tag{5}$$

$$\angle G_{PR}(j\omega) = \arctan\frac{2\omega_{PRc}\omega}{\omega_h^2-\omega^2}\left(1+\frac{K_{rh}}{K_{ph}}\right)-\arctan\frac{2\omega_{PRc}\omega}{\omega_h^2-\omega^2} \tag{6}$$

To reduce the total harmonic distortion (THD) of grid current below 5% as mentioned in the IEEE1547 standard for interconnecting distributed generations and mitigate odd harmonics of 3rd, 5th, and 7th orders, a harmonic compensator (HC) is cascaded with the PR controller in (4). The transfer function of the HC and PR controller is thus given as follows:

$$G_{PR}(s) = G_{PR1}(s)+G_{PR3}(s)+G_{PR5}(s)+G_{PR7}(s) = \sum_{h=1,3,5,7,\ldots} K_{ph} + \sum_{h=1,3,5,7,\ldots}\frac{2K_{rh}\omega_{PRc}s}{s^2+2\omega_{PRc}s+\omega_h^2} \tag{7}$$

To analyze the transfer function of the system in s-domain, the current loop with two feedback methods using grid-current feedback and inverter-current feedback is derived and shown in Fig. 5.

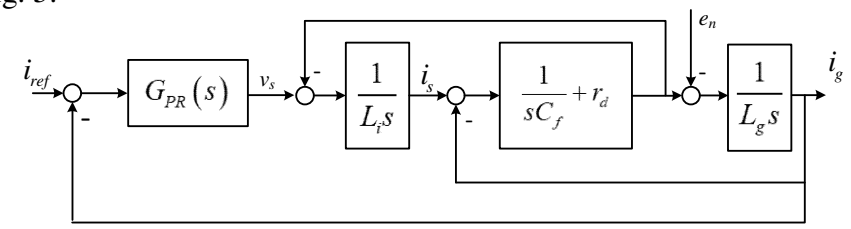

a. Grid-current feedback

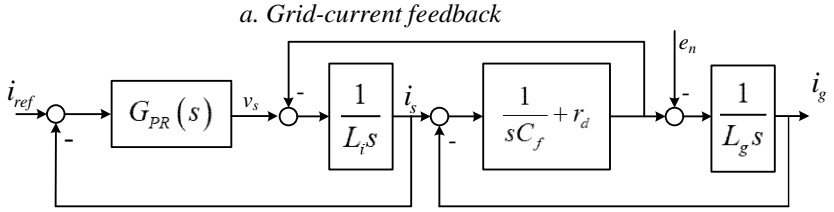

b. Inverter-current feedback

Figure 5. The s-domain block diagrams of LCL-type grid-connected VSIs with different current feedback controls.

At the cross-over frequency, the magnitude-frequency response of the system is unity, and the controller gain K_{ph} of PR controllers is determined as follows:

$$\begin{aligned}&\left(\sum_{h=1,3,5,7...}\left|G_{PRh}(j\omega)\right|_{\omega=\omega_C}\right)\left|G_{vi}(j\omega)\right|_{\omega=\omega_C}=1\\&\rightarrow\sum_{h=1,3,5,7...}K_{ph}\approx\frac{1}{\left|G_{vi}(j\omega)\right|_{\omega=\omega_C}}\end{aligned}\tag{8}$$

The unity gain of the PR controller can be divided among harmonic orders of grid voltage. For example, if the tracking for the fundamental current and low order harmonics is given a higher priority compared to other harmonic orders, $\left|G_{PR1}(j\omega)\right|_{\omega=\omega_C}$ $\left|G_{vi}(j\omega)\right|_{\omega=\omega_C}$ is given the highest value while the corresponding quantities for tracking 3th, 5th, and 7th can be set to smaller values.

he PM of the PR controller is determined based on the desired value *PM* of the system's open-loop transfer function the cross-over frequency ω_c [17], which is given as follows:

$$PM=\angle G_{PRh}(j\omega)\big|_{\omega=\omega_C}+\angle G_{vi}(j\omega)\big|_{\omega=\omega_C}+180^0\tag{9}$$

Since the PM of system is limited by its minimum and maximum values, the PM of the PR controller is thus calculated as follows:

$$\begin{aligned}&\min(PM)-\left[\angle G_{vi}(j\omega)\big|_{\omega=\omega_C}+180^0\right]\le\angle G_{PRh}(j\omega)\big|_{\omega=\omega_C}\le\max(PM)-\left[\angle G_{vi}(j\omega)\big|_{\omega=\omega_C}+180^0\right]\\&\text{or:}\qquad A_1\le\angle G_{PRh}(j\omega)\big|_{\omega=\omega_C}\le A_2\end{aligned}\tag{10}$$

where:

$$\begin{aligned}A_1&=\min(PM)-\left[\angle G_{vi}(j\omega)\big|_{\omega=\omega_C}+180^0\right]\\A_2&=\max(PM)-\left[\angle G_{vi}(j\omega)\big|_{\omega=\omega_C}+180^0\right]\end{aligned}\tag{11}$$

Substituting (6) into (11), the lower and upper thresholds of K_{rh} are determined as follows:

$$\begin{aligned}&A_1\le\arctan\left[\frac{2\omega_{PRc}\omega_c}{\omega_h^2-\omega_c^2}\left(1+\frac{K_{rh}}{K_{ph}}\right)\right]-\arctan\frac{2\omega_{PRc}\omega_c}{\omega_h^2-\omega_c^2}\le A_2\\&\rightarrow K_{ph}\left\{\frac{\omega_h^2-\omega_c^2}{2\omega_{PRc}\omega_c}\tan\left[A_1+\arctan\left(\frac{2\omega_{PRc}\omega_c}{\omega_h^2-\omega_c^2}\right)\right]-1\right\}\le K_r\le K_p\left\{\frac{\omega_h^2-\omega_c^2}{2\omega_{PRc}\omega_c}\tan\left[A_2+\arctan\left(\frac{2\omega_{PRc}\omega_c}{\omega_h^2-\omega_c^2}\right)\right]-1\right\}\\&\rightarrow K_{ph}\left\{\frac{1}{M}\tan\left[A_1+\arctan(M)\right]-1\right\}\le K_{rh}\le K_{ph}\left\{\frac{1}{M}\tan\left[A_2+\arctan(M)\right]-1\right\}\\&\rightarrow\min(K_{rh})\le K_{rh}\le\max(K_{rh})\end{aligned}\tag{12}$$

where $M=\dfrac{2\omega_{PRc}\omega_c}{\omega_h^2-\omega_c^2}$ and the fundamental frequency of the grid voltage is assumed to vary in the range of ±1Hz, i.e. $\omega_{PRc}=2\pi$ (rad/s). The relation between the cross-over frequency f_c, the sampling frequency f_s, and the resonant frequency of LCL filter f_{res} is shown in (13), in which f_c is selected to be far lower than f_s and much smaller than f_{res} [15].

$$\begin{cases} f_c \le \dfrac{f_s}{10} \\ \dfrac{f_s}{4} \le f_{res} \le \dfrac{f_s}{2} \end{cases} \tag{13}$$

3.2. The designed non-ideal PR controller in discrete domain

The discretization method for the non-ideal PR controller proposed in Section 3.1 is modified from the method applied for ideal PR controllers in [18], which is based on the positive- and negative-sequence transfer fucntions of the classical PI controller. Since the time delay is T_d due to the PWM update and the ZOH (Zero Order Hold), the phase is varied and the peaks existing around the resonant frequency are amplified [19]. Thus, several techniques propose the delay compensation to mitigate the effect of the delay. The delay can be compensated by adding a lead angle $\theta_d = \omega_h N T_s$ to the inverse Park transform angle, where N is an integer representing the number of periods to be compensated [18]. In this paper, N is set to 1.

The positive- and negative-sequence transfer functions of the classic PI controller in the SRF are given as follows:

$$G_{PI}^{-}(s) = K_{pih} + \frac{K_{rh}}{1+\left(\dfrac{s+j\omega_h}{\omega_{PRc}}\right)} e^{-j\theta_d} \tag{14}$$

$$G_{PI}^{+}(s) = K_{pih} + \frac{K_{rh}}{1+\left(\dfrac{s-j\omega_h}{\omega_{PRc}}\right)} e^{+j\theta_d} \tag{15}$$

Therefore, the transfer function of the PR controller with the delay compensation can be obtained as follows:

$$\begin{aligned} G_{PR}^{c}(s) &= G_{PI}^{-}(s) + G_{PI}^{+}(s) \\ &= 2K_{pih} + K_{rh} \frac{\omega_{PRc}\cos(\theta_d)s + \left[\omega_{PRc}^2\cos(\theta_d) - h\omega_1\sin(\theta_d)\omega_{PRc}\right]}{s^2 + 2\omega_{PRc}s + \left[\omega_{PRc}^2 + \omega_h^2\right]} \end{aligned} \tag{16}$$

Since $\omega_{PRc} \ll \omega_h$, (16) can be rewritten as follows:

$$G_{PR}^{c}(s) \approx K_{ph} + 2K_{rh} \frac{\omega_{PRc}\cos(\theta_d)s - h\omega_1\sin(\theta_d)\omega_{PRc}}{s^2 + 2\omega_{PRc}s + \omega_h^2} \tag{17}$$

The PR controller expressed in (16) and (17) consists of double integrators with direct and feedback components. To avoid an algebraic loop during the discrete implementation, it is suggested that the direct integrator is discretized using the forward method while the feedback integrator is discretized using the backwards method [20], [21].

$$G_{PR}^{c}(s) = K_{ph} + 2K_{rh} \frac{\omega_{PRc}\cos(\theta_d)\dfrac{1}{s} - \omega_h\sin(\theta_d)\omega_{PRc}\dfrac{1}{s}\dfrac{1}{s}}{s^2 + 2\omega_{PRc}\dfrac{1}{s} + \omega_h^2\dfrac{1}{s}\dfrac{1}{s}} \tag{18}$$

Substituting $s \approx \frac{z-1}{T_s}$ and $s \approx \frac{z-1}{zT_s}$ into equation (18), the proposed PR controller in z–domain can be written as follows:

$$G_R^d(z) \approx K_{ph} + 2K_{rh} \frac{\omega_{PRc} \cos\theta_d \frac{T_s}{z-1} - \omega_h \omega_{PRc} \sin\theta_d \frac{T_s}{z-1}\frac{zT_s}{z-1}}{1 + 2\omega_{PRc}\frac{T_s}{z-1} + \omega_h^2 \frac{T_s}{z-1}\frac{zT_s}{z-1}}$$
$$\leftrightarrow G_R^d(z) \approx K_{ph} + 2K_{rh} \frac{\left(\omega_{PRc}\cos\theta_d T_s - T_s^2 \omega_h \omega_{PRc} \sin\theta_d\right) z - \omega_{PRc}\cos\theta_d T_s}{z^2 + \left(\omega_h^2 T_s^2 + 2\omega_{PRc}T_s - 2\right) z + \left(1 - 2\omega_{PRc}T_s\right)} \quad (19)$$

4. Results and discussion

4.1. Off-line simulation

The simulation of the proposed PR controllers for LCL-type grid-connected VSIs in distorted grid voltages is carried out in Matlab/Simulink/Simpower. The parameters of the test system are shown in Table I.

Table I. Parameters of the single-phase LCL-type grid-connected VSI

Rated power	3 kW
Grid voltage (RMS/Frequency)	220 V/50 Hz ± 1Hz
DC-link voltage	400 V
Switching frequency	10 kHz
Grid and Converter side inductance	L_g = 0.7 mH, L_i = 1.2 mH
Filter capacitance	C_f = 6.6 μF
Damping resistor	r_d=8 Ω

With the filter parameters shown in Table I, the desired phase margin PM is between 30^0 and 45^0, and the cross-over frequency is 900 Hz. The 3rd, 5th and 7th harmonics added to the grid voltage are about 5%, 6% and 5%, respectively, so that the THD is 9.27%. Besides, the variation of grid frequency is selected to be ±1Hz at 0.1s and 0.2s. For tracking the fundamental frequency, $\left|G_{PR1}(j\omega)\right|_{\omega=\omega_c}\left|G_{vi}(j\omega)\right|_{\omega=\omega_c} = 0.4$, while the corresponding quantities for tracking 3th , 5th , and 7th are set to 0.15, 0.3, 0.15, respectively. The parameters of the PR controllers are calculated using the method described in Section 3, and the calculated parameters of PR controller for each harmonic order is shown in Table II. The Bode diagram that represents the characteristics of the current control loop with the implementation of the PR controller are shown in Fig. 6. The current loop is shown to be stable.

Table II. The parameters of the designed PR controller for each harmonic order

	K_p	[Min(K_{rh}), Max(K_{rh})]	[Min(PM), Max(PM)]	f_c
Grid-current feedback	K_{p1} = 0.0102 K_{p3} = 0.0038 K_{p5} = 0.0077 K_{p7} = 0.0038	K_{r1}= [2.399÷ 4.2231] K_{r3} = [0.8774÷ 1.5445] K_{r5} = [1.6657÷ 2.9325] K_{r7} = [0.7661÷ 1.3488]	[31.6^0, 45.4^0]	[1kHz, 1.14kHz]
Inverter-current feedback	K_{p1} = 0.0118 K_{p3} = 0.0044 K_{p5} = 0.0089 K_{p7} = 0.0044	K_{r1}= [3.0971÷5.3612] K_{r3} = [1.1327÷1.9608] K_{r5} = [2.1505÷3.7228] K_{r7} = [0.9891÷1.7124]	[34.1^0, 46.5^0]	[996Hz, 1.1kHz]

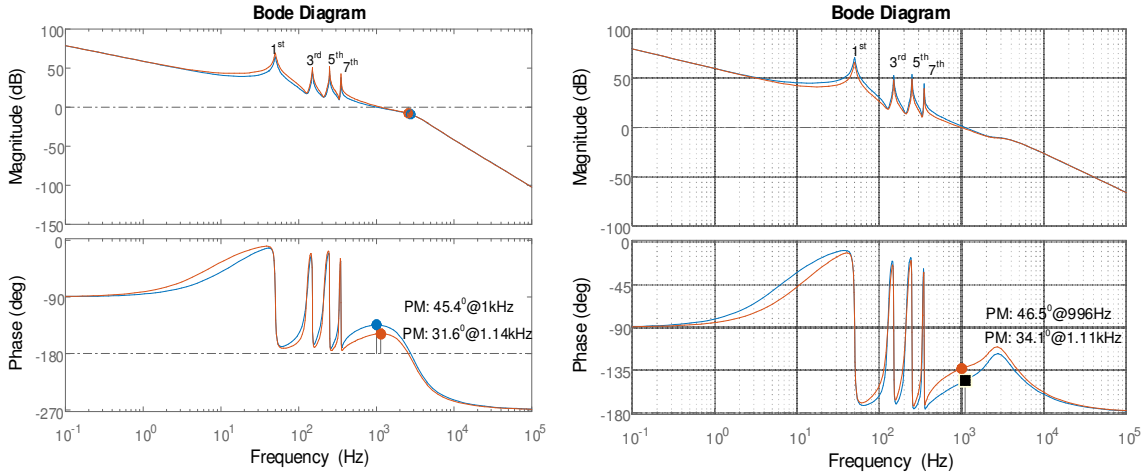

a. Grid-current feedback. b. Inverter-current feedback.

Figure 6. Bode diagrams of open-loop transfer function

Simulations are carried out to observe the effect of harmonic compensation on the grid current with grid current feedback and inverter current feedback method, when grid voltage contains the aforementioned odd harmonics of 3rd, 5th, and 7th. To achieve the synchronization in single–phase system with high quality, we used a phase-locked loop (PLL) algorithm based on a second-order generalized integrator phase-locked loop (SOGI PLL) [22]. Unipolar pulse-width-modulation technique is also implemented to control the switching of the IGBT switches of the single-phase VSI.

When the grid-current feedback is applied, the 3rd, 5th, and 7th harmonics in the grid current are about 0.74%, 0.56%, 0.6% of the reference value of 10A peak, respectively. The corresponding TDH of the grid current is 1.87%, which is compliant with the IEEE and IEC standards. The 3rd, 5th, and 7th harmonics of the inverter current are about 1.56%, 2.01%, 1.66%, respectively, while its THD is 3.38%. The performances of the system with the maximum and minimum PMs as reported in Table II are shown in Fig. 7.

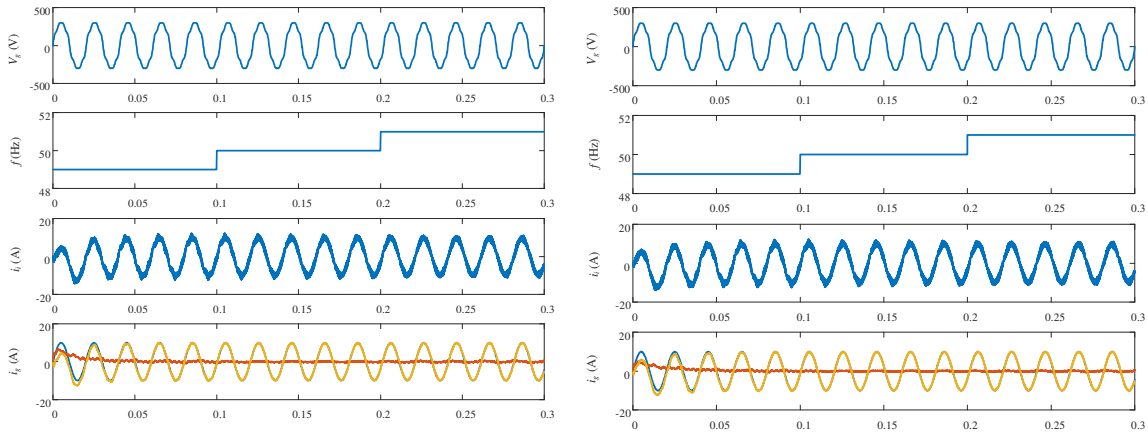

a. PM = 45.4^0 at 1.14 kHz b. PM = 31.6^0 at 1 kHz

Figure 7. Performance of the system when applying grid-current feedback.

When the inverter-current feedback is applied, the 3rd, 5th and 7th harmonics of the grid-current are about 0.68%, 2.02%, 3.18% of the reference value of 10A peak, respectively. The corresponding THD of the grid current is 4.11%. Although this value still satisfies the IEEE and IEC standards, the quality of the grid current is worse than that when employing grid-current feedback. The 3rd, 5th, and 7th harmonics of the inverter current are

about 0.83%, 0.32%, 0.77%, respectively, while its THD is 1.88%. The performances of the system with the maximum and minimum PMs as reported in Table II are shown in Fig. 8.

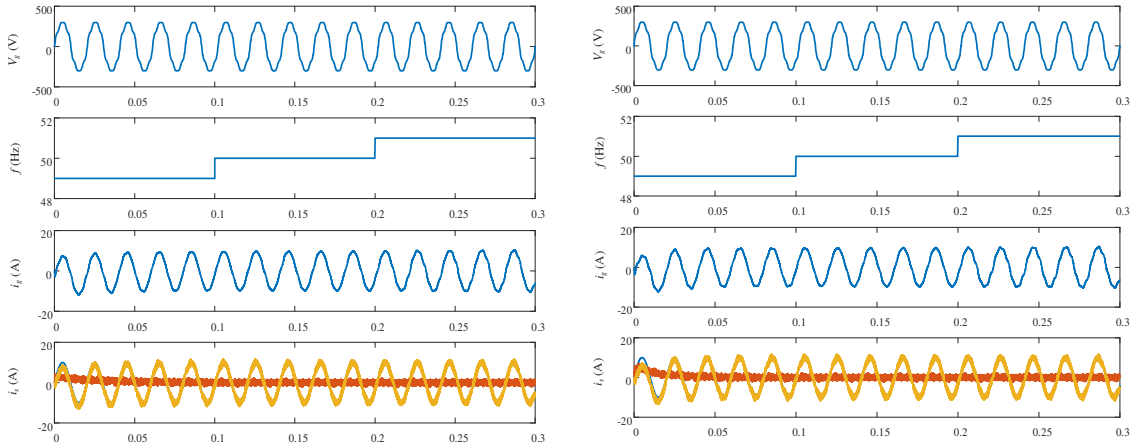

b. PM = 46.5^0 at 1.1 kHz b. PM = 34.1^0 at 996 Hz

Figure 8. Performance simulation in inverter-current feedback.

4.2. Hardware-in-the-loop experimental results

To verify the proposed design of PR current controllers for LCL-type grid-connected VSIs and conveniently simulate the aforementioned non-ideal operating conditions of grid voltage, this paper uses a standard Typhoon HIL device shown in Fig. 9 [23-25]. This device consists of an HIL 402 card that simulates a grid voltage source, an LCL filter, and a single-phase VSI using IGBTs. The system hardware is simulated in real time using the HIL platform with a time step of 1 μs, which closely represents the real physical model. The pulse-width-modulation carrier frequency is 10 kHz. The current regulators as well as the PLL algorithm are implemented in DSP TMS320F2808 card.

Figure 9. The hardware setup for the HIL platform.

The grid voltage contains 3rd, 5th, and 7th harmonics with a THD of 9.27%, as shown in Fig. 10. The grid voltage and currents are measured using Oscilloscope HAMEG – 200MHz at the test points in HIL DSP interface of Typhoon.

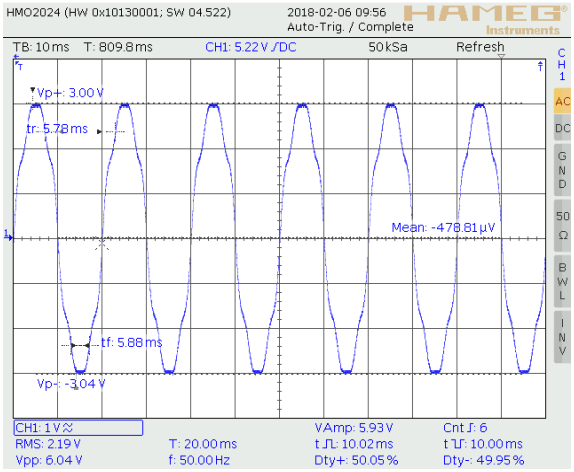

a. Waveform of grid voltage

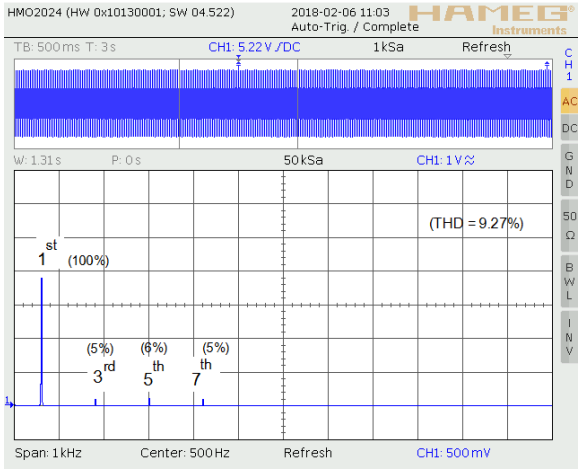

b. FFT analysis waveform of grid voltage

Figure 10. The grid voltage in HIL exprimentation.

The HIL experimental results with the grid-side current feedback is applied are shown in Fig. 11. The 3rd, 5th, and 7th harmonics of the grid current are reduced to 1.38%, 0.93%, and 0.92%, respectively, while its THD is 2.14%. The 3rd, 5th, and 7th harmonics of the inverter current are about 1.02%, 1.8%, and 1.63%, respectively, while its THD is 2.79%.

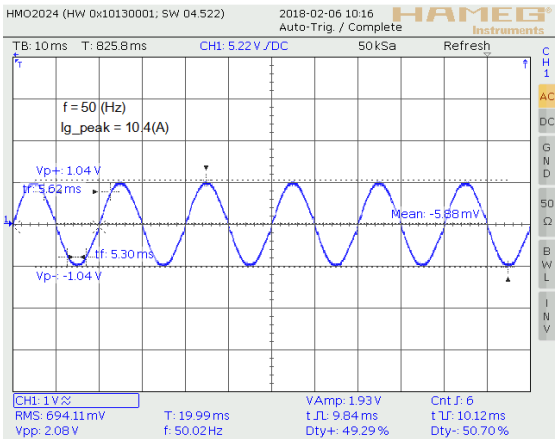

a. Waveform of grid-side current

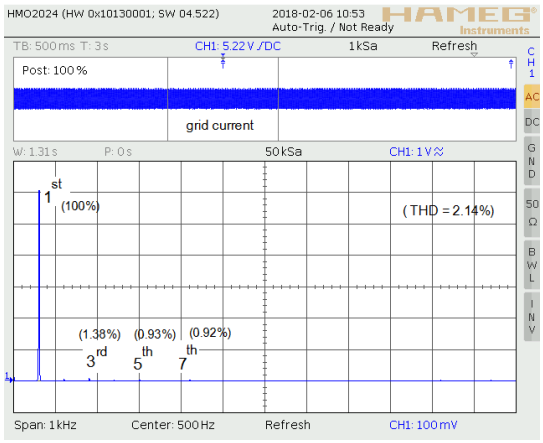

b. The spectrum of grid-side current

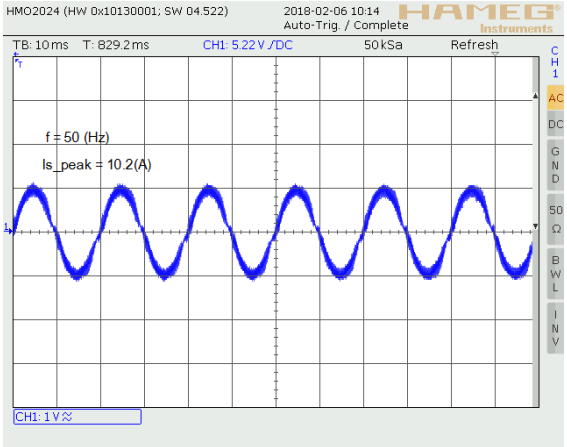

c. Waveform of inverter-side current

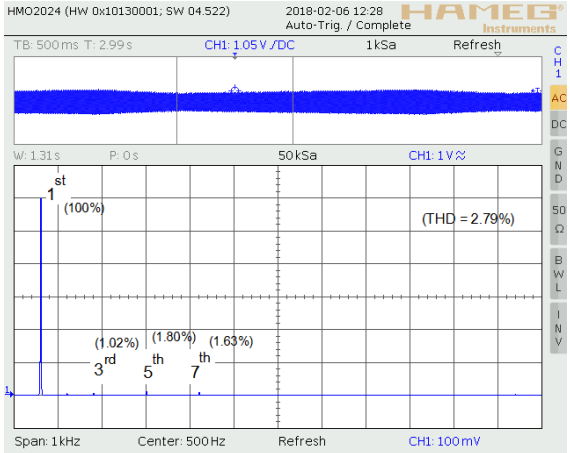

d. The spectrum of inverter-side current

Figure 11. The HIL experimental results with grid-current feedback.

When the inverter-side current feedback is applied, the HIL experimental results are shown in Fig. 12. The 3rd, 5th, and 7th harmonics of the grid current are about 2.15%, 2.97%, and 3.81%, respectively, while its THD is 5.62%. This result fails to comply with the IEEE standard. The 3rd, 5th, and 7th harmonics of the inverter current are about 1.17%, 1.71%, and 1.69%, respectively, while its THD is 3.2%.

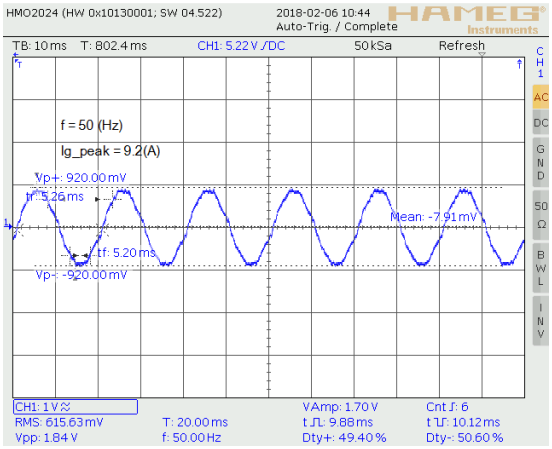

a. Waveform of grid-side current

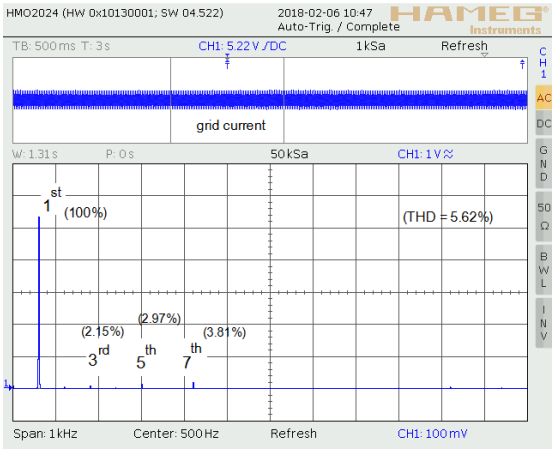

b. The spectrum of grid-side current

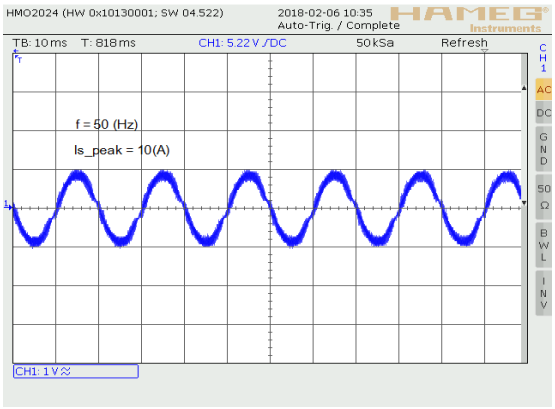

c. Waveform of inverter-side current

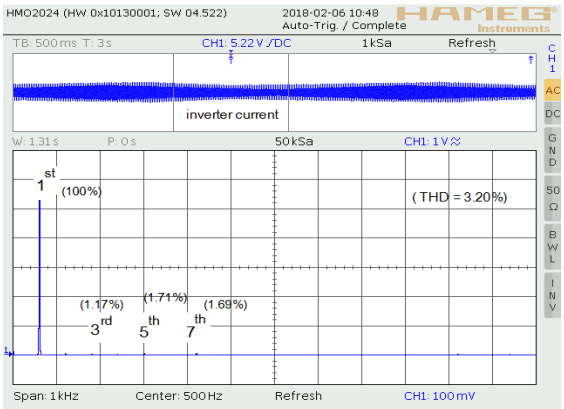

d. The spectrum of inverter-side current

Figure 12. The HIL experimental results with inverter-side current feedback.

5. Conclusion

This paper proposes a systematic and generalized design method for a non-ideal PR current controller used in LCL-type grid-connected VSIs. The designed PR controller contains multiple resonant components to eliminate the effect of grid voltage harmonics and the variation of the fundamental grid frequency. The parameters of the PR controller are determined in the frequency domain, taking into account the full third-order model of LCL filters and the limits of system phase margin to guarantee system stability. The proposed method is applicable for both inverter-current and grid-current feedbacks and thus for both passive and active damping approaches. The proposed design is verified by off-line simulation and HIL experiments with the VSI is connected to a distorted grid voltage. The results show that the designed PR controller is able to reduce the low-order harmonics and THD of the grid current. Specifically, the THD of the grid current when employing the grid-current feedback approach is only 1.87% and 2.14% for off-line simulation and HIL experiment, respectively. When inverter-current feedback is used, these THD values are 4.11% and 5.62%. Therefore, for practical applications of LCL-type single-phase VSIs with

distorted grid voltage, grid-current feedback should be implemented to improve the quality of grid current.

Acknowledgment

This research is funded by the Hanoi University of Science and Technology (HUST) under project number T2017-PC-109.

References

[1] K. Jalili and S. Bernet, Design of LCL Filters of Active-Front-End Two-Level Voltage-Source Converters, *IEEE Transactions on Industrial Electronics*, vol. 56, no. 5, pp. 1674-1689, May 2009.

[2] T. F. Wu, M. Misra, L. C. Lin and C. W. Hsu, An Improved Resonant Frequency Based Systematic LCL Filter Design Method for Grid-Connected Inverter, *IEEE Transactions on Industrial Electronics*, vol. 64, no. 8, pp. 6412-6421, Aug. 2017.

[3] S. Jayalath and M. Hanif, Generalized LCL-Filter Design Algorithm for Grid-Connected Voltage-Source Inverter, *IEEE Transactions on Industrial Electronics*, vol. 64, no. 3, pp. 1905-1915, March 2017.

[4] C. Zhang, T. Dragicevic, J. C. Vasquez and J. M. Guerrero, Resonance damping techniques for grid-connected voltage source converters with LCL filter - A review, *2014 IEEE International Energy Conference (ENERGYCON)*, Cavtat, 2014, pp. 169-176.

[5] Y. Han, Z. Li and J. M. Guerrero, Dynamic evaluation of LCL-type grid-connected inverters with different current feedback control schemes, *2015 9th International Conference on Power Electronics and ECCE Asia* (ICPE-ECCE Asia), Seoul, 2015, pp. 391-396.

[6] Z. Xin, X. Wang, P. C. Loh and F. Blaabjerg, Grid-Current-Feedback Control for LCL-Filtered Grid Converters With Enhanced Stability, *IEEE Transactions on Power Electronics*, vol. 32, no. 4, pp. 3216-3228, April 2017.

[7] A. J. Xu, B. S. Xie, C. J. Kan and D. L. Ji, An improved inverter-side current feedback control for grid-connected inverters with LCL filters, *2015 9th International Conference on Power Electronics and ECCE Asia* (ICPE-ECCE Asia), Seoul, 2015, pp. 984-989.

[8] X. Wang, F. Blaabjerg and P. C. Loh, Grid-Current-Feedback Active Damping for LCL Resonance in Grid-Connected Voltage-Source Converters, *IEEE Transactions on Power Electronics*, vol. 31, no. 1, pp. 213-223, Jan. 2016.

[9] Hu, Guozhen & Chen, Changsong & Shanxu, Duan. (2013). New Active Damping Strategy for LCL-Filter-Based Grid-Connected Inverters with Harmonics Compensation. *Journal of Power Electronics*. 13. .10.6113/JPE.2013.13.2.287.

[10] Xu, Jinming & Xie, Shaojun & Zhang, Binfeng. (2016). Stability Analysis and Improvement of the Capacitor Current Active Damping of the LCL Filters in Grid-Connected Applications. *Journal of power electronics*. 16. 1565-1577. 10.6113/JPE.2016.16.4.1565.

[11] Xu, Jinming & Xie, Shaojun & Tang, Ting. (2013). Systematic Current Control Strategy with Pole Assignment for Grid-Connected LCL-Filtered Inverters. *Journal of Power Electronics*. 13. . 10.6113/JPE.2013.13.3.447.

[12] R. Chattopadhyay, A. De and S. Bhattacharya, Comparison of PR controller and damped PR controller for grid current control of LCL filter based grid-tied inverter under frequency variation and grid distortion, *2014 IEEE Energy Conversion Congress and Exposition (ECCE)*, Pittsburgh, PA, 2014, pp. 3634-3641.

[13] R. Teodorescu, F. Blaabjerg, M. Liserre and P. C. Loh, Proportional-resonant controllers and filters for grid-connected voltage-source converters, *IEE Proceedings - Electric Power Applications*, vol. 153, no. 5, pp. 750-762, September 2006.

[14] G. Shen, X. Zhu, J. Zhang, and D. Xu, A new feedback method for PR current control of LCL-filter-based grid-connected inverter, *IEEE Trans. Ind. Electron.*, Vol. 57, No. 6, pp. 2033-2041, Jun. 2010.

[15] Zhang, Ningyun & Tang, Houjun & Yao, Chen. (2014). A Systematic Method for Designing a PR Controller and Active Damping of the LCL Filter for Single-Phase Grid-Connected PV Inverters. *Energies*. 7. 3934-3954. 10.3390/en7063934.

[16] Daniel Zammit, Cyril Spiteri Staines, Maurice Apap, John Licari, Design of PR current control with selective harmonic compensators using Matlab, *Journal of Electrical Systems and Information Technology*, Volume 4, Issue 3, 2017, Pages 347-358, ISSN 2314-7172, https://doi.org/10.1016/j.jesit.2017.01.003.

[17] Y. Song, J. Wang and A. Monti, Design of systematic parameter tuning approaches for multiple proportional-resonance AC current regulator, *2015 IEEE 6th International Symposium on Power Electronics for Distributed Generation Systems (PEDG),* Aachen, 2015, pp. 1-7.

[18] M. S. Lima, L. A. d. S. Ribeiro and J. G. de Matos, Comparison analysis of resonant controllers in discrete domain taking into account the computational delay, 2015 IEEE 13th Brazilian Power Electronics Conference and 1st Southern Power Electronics Conference (COBEP/SPEC), *Fortaleza*, 2015, pp. 1-6.

[19] Zipeng Li, Aiting Jiang, Pan Shen, Yang Han and J. M. Guerrero, Resonance damping and parameter design method for LCL-LC filter interfaced grid-connected photovoltaic inverters, 2016 IEEE 8th International Power Electronics and Motion Control Conference (IPEMC-ECCE Asia), *Hefei, 2016*, pp. 1581-1586.

[20] R. Teodorescu, F. Blaabjerg, U. Borup and M. Liserre, "A new control structure for grid-connected LCL PV inverters with zero steady-state error and selective harmonic compensation," *Applied Power Electronics Conference and Exposition, 2004. APEC '04. Nineteenth Annual IEEE*, 2004, pp. 580-586 Vol.1.

[21] F. de Bosio, L. A. d. S. Ribeiro, M. S. Lima, F. Freijedo, J. M. Guerrero and M. Pastorelli, "Inner current loop analysis and design based on resonant regulators for isolated microgrids," *2015 IEEE 13th Brazilian Power Electronics Conference and 1st Southern Power Electronics Conference (COBEP/SPEC)*, Fortaleza, 2015, pp. 1-6.

[22] R. Teodorescu, M. Liserre, and P. Rodrguez, Grid converters for photovoltaic and wind power systems. *John Wiley, Ltd*, 2011.

[23] Typhoon HIL, Inverter Testing & Pre-certification with HIL Testing. *Available: https://www.typhoon-hil.com/applications/converter-testing*.

[24] Z. R. Ivanović, E. M. Adžić, M. S. Vekić, S. U. Grabić, N. L. Čelanović and V. A. Katić, HIL Evaluation of Power Flow Control Strategies for Energy Storage Connected to Smart Grid Under Unbalanced Conditions, *IEEE Transactions on Power Electronics*, vol. 27, no. 11, pp. 4699-4710, Nov. 2012.

[25] M. S. Vekić, S. U. Grabić, D. P. Majstorović, I. L. Čelanović, N. L. Čelanović and V. A. Katić, Ultralow Latency HIL Platform for Rapid Development of Complex Power Electronics Systems, *IEEE Transactions on Power Electronics*, vol. 27, no. 11, pp. 4436-4444, Nov. 2012.